EPJ Web of Conferences **21**, 08005 (2012)
DOI: 10.1051/epjconf/20122108005

Effect of alpha-Q-value on reaction dynamics at ≈ 4-7 AMeV

Abhishek Yadav[1,a], Vijay R. Sharma[1], Pushpendra P. Singh[2], Devendra P. Singh[1], Unnati[1], Manoj K. Shamra[3], R. Kumar[4], B. P. Singh[1], R. Prasad[1], and R. K. Bhowmik[4,b]

[1] Acc. Lab., Department of Physics, A. M. University, Aligarh - 202 002, India
[2] GSI Helmholtz Centre for Heavy Ion Research GmbH, D-64291 Darmstadt, Germany
[3] S. V. College, Agra University, Agra, India
[4] NP-Group, Inter-University Accelerator Center, New Delhi - 110 067, India

Abstract. This paper deals with the dependence of incomplete fusion reaction dynamics on various entrance channel parameters, specially, the alpha-Q-value effect. The excitation functions for several radio-nuclides formed in ^{13}C+^{159}Tb interactions at ≈ 4-7 AMeV have been measured using activation technique followed by γ-spectroscopy. The experimentally measured excitation functions have been analyzed in the framework of statistical model code PACE4. A sizeable contribution of incomplete fusion has been delineated in the production of α-emitting channels in reference to the Monte Carlo simulation based statistical model code PACE4. For better insights into the onset and strength of incomplete fusion, the incomplete fusion strength function has been deduced as a function of various entrance channel parameters. A significant amount of incomplete fusion contribution has been observed at slightly above barrier energies, and found to increase smoothly with incident projectile energy. Present results have also been compared with the results obtained in the interactions of ^{16}O and ^{12}C with same target ^{159}Tb, to probe the dependence of incomplete fusion on projectile, specially, on the binding energy & alpha-Q-value. The present work in light of previous data hints that instead of binding energy, the alpha-*Q*-value of the projectile is a parameter which influences the in-complete fusion reaction dynamics.

1 Introduction

Incomplete fusion (ICF) reactions, as recognized since mid-sixties by the very first experimental observation[1] of energetic α-particles emitted very copiously in heavy-ion (HI)-induced reactions at energies > 10.6 AMeV, are the collisions where, besides the formation of a fusion-like nucleus and its decay, forward peaked "fast α-particles" have been observed. The ICF is still an active area of investigations due to complex nature of in-complete mass transfer and its ambiguous dependence on various entrance channel parameters viz., projectile type/energy, imparted input angular momentum (ℓ) to the system, α-break-up energy (Q_α), mass-asymmetry of the interaction partners (μ_A=A_T/A_{T+P}), deformations of interaction partners etc. An outstanding theoretical challenge, emerged after the observation of "fast α-particles", is to model the ICF processes. Several approaches have been adopted to understand the ICF-reaction processes [2–16]. In the most commonly used model, proposed by Siwek-Wilczynska et a1.[21], the concept of generalized critical angular momentum (ℓ) has been used. According to this model, if the entrance channel angular momentum exceeds the critical limit ℓ_{crit} for complete fusion, the fusion can not occur unless a part of the projectile (P^S) is emitted which carries away the excess of angular momentum. The remainder of the projectile (P^P) has now a resulting angular momentum lower than its own critical limit for fusion with the target ($\ell_{eff} \leq \ell_{crit}^{P^P+T}$). This model has been completed by Wilczynski et a1.[25], by the addition of a "sum-rule" formalism applied to complete and incomplete fusion reactions. Quantum mechanical models such as the continuum discretized coupled channels model (CDCC) and the time-dependent wave packet method have also been proposed, which are unable to separate out the incomplete and complete fusion contributions. However, A. Diaz-Torres et al. in his recent paper[3] has presented a classical dynamical model that treats breakup stochastically for low energy reactions of weakly bound nuclei. It may, further, be pointed out that the aforementioned models/theories, generally, have been used to fit the experimental data obtained at energies ≥ 10.5 AMeV or so. However, in general, none of the proposed models is able to fit the experimental data obtained at relatively low bombarding energies i.e., ≈ 4-7 AMeV. As such, due to the unavailability of any reliable theoretical model to ex-

[a] e-mail: abhishekyadav117@gmail.com
[b] Present Address: Department of Pure and Applied Physics, Guru Ghasidas University, Koni, Bilaspur - 495009 (CG), India

plain the emission of fast PLFs associated with ICF at energies ≈ 4-7 AMeV, the study of ICF is still an active area of investigations.

The ^{12}C, ^{16}O and ^{20}Ne, which are considered to have α-cluster structure, beams have been used in most of the previous studies. In fact the cluster structure has been suggested as one of the factors leading to forward peaked alpha particles in ICF reactions. Some amount of experimental data is now available but no systematic studies have been carried out to ascertain this aspect and more results are necessary. As such, a program has been undertaken to carry out some conclusive experiments using ^{13}C, ^{14}N and ^{18}O beams on different targets, which may provide us a rich data set to understand the underlying dynamics. The present work is the first step in this direction, where, the excitations functions of ^{12}C+^{159}Tb [14] and ^{13}C+^{159}Tb (present work) systems at energies ≈ 4-7 AMeV have been measured and analyzed in the frame-work of equilibrated compound nucleus decay. The ICF cross sections for other systems have been compared to study convincingly the effect of different entrance-channel parameters on the said reaction dynamics. The structure of the paper is as follows; the section-2 deals with the experimental methodology, while the analysis of experimental excitation functions in terms of CN-model is given in section-3. While, the summary of the present work is given in last section of the paper.

2 Experimental details and methodology

The experiments have been performed using the ^{13}C beam delivered from the 15UD-Pelletron at the Inter University Accelerator Center (IUAC), New Delhi, India using the off-line γ-ray spectroscopy [11,12]. The isotopically pure, self-supporting ^{159}Tb targets (t_m ≈ 1.2-2.8 mg/cm^2) and the *Al*-foils (t_m ≈ 1.5-2.5 mg/cm^2), served as energy degrader as well as catcher foils of sufficient thickness to stop the recoiling residues produced during the interaction, were prepared using the rolling technique. In order to achieve wide energy range in a single irradiation, energy degradation technique has been used. In the present experiment five stacks, each having three target-catcher foil assemblies were irradiated at energies ≈ 58, 70, 73, 85 and 88 MeV. Keeping the half-lives of interest in mind, irradiations were carried out for ≈ 9-11 h duration for each stack. The Pelletron crew provided a nearly constant beam current ≈ 30 nA throughout the irradiations. A Faraday cup, which was placed behind the target-catcher foil assembly, was used to measure the integrated beam current, for every 120 s, so as to correct for the variation in the beam intensity during the irradiation time, which are particularly significant for short-lived radio-nuclides. The activities produced in each target-catcher foil assembly have been recorded using a high resolution HPGe detector coupled to a

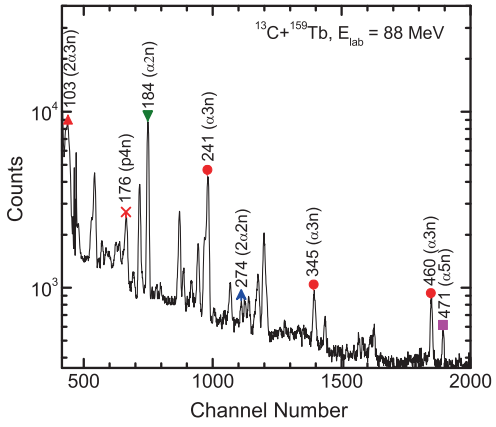

Fig. 1. Typical γ-ray spectrum showing γ-lines of different radio-nuclides populated via CF and/or ICF in ^{13}C+^{159}Tb interations at projectile energy ≈ 88MeV.

PC through CAMAC based data acquisition software CANDLE (Collection & Analysis of Nuclear Data using Linux nEtwork)[28]. A typical γ-ray spectrum obtained at ≈ 87.62 ± 0.40 MeV beam energy is shown in Fig.1. The detector used in these experiments was pre-calibrated both for energy as well as efficiency using various standard γ-sources such as ^{60}Co, ^{133}Ba and ^{152}Eu. It may, however, be pointed out that most of the γ-rays of interest for the expected residues lie in this energy range. The energy resolution of the detector was ≈2.5 keV at the 1408 keV γ-line of ^{152}Eu. A 50Hz pulser was used to determine the dead time. The detector-sample separation was adjusted such as to kept the dead-time below 10% during the counting so as to minimize the pile up effects. The efficiency calibration of the detector in the specified geometry was carried out using a standard ^{152}Eu source of known strength at various source-detector separations in order to wash out the solid angle effect and to increase the accuracy in the measurement of cross-section.

2.1 Identification of reaction products

In order to determine the production cross-section of these residues, first of all it is desirable to identify the various reaction products via thier characteristic γ-lines. However, the confirmation of the evaporation residues were made by measureing their decay half-lives. The reaction residues identified using the assignment of characteristic γ-radiations and decay curve analysis are given in Tables-I, alongwith their spectroscopic properties which has been taken from the Table of Isotopes[29].

Table 1. List of identified reaction residues (channels) with their spectroscopic properties

Residue	$T_{1/2}$	J^{π}	E_{γ}(keV)	I^{γ} (%)
^{169}Lu(3n)	34.06 hrs	$7/2^{+}$	191.21	20.6
^{168}Lu(4n)	5.5 min	3^{+}	198.86	180.0[a]
			228.58	70.0[a]
^{168m}Lu(4n)	6.7 min	6^{-}	198.86	180.0[a]
			228.58	70.0[a]
^{167}Lu(5n)	51.5 min	$7/2^{+}$	213.21	3.5
^{167}Yb(p4n)	17.5 min	$5/2^{-}$	176.2	20.4
			177.26	2.7
^{166}Tm(α2n)	7.70 hrs	2^{+}	184.41	16.1
			215.19	5.24
^{165}Tm(α3n)	30.06 hrs	$1/2^{+}$	242.85	35
			346.75	3.9
			356.44	3.7
			460.12	3.7
^{163}Tm(α5n)	1.81 hrs	$1/2^{+}$	190.07	1.28
			239.67	4.1
			471.29	3.8
^{162}Ho(2α2n)	15.0 hrs	1^{+}	185.20	28.6
^{162m}Ho(2α2n)	67.0 hrs	6^{-}	185.20	0.42
^{161}Ho(2α3n)	2.48 hrs	$7/2^{-}$	103.03	3.6
^{160}Ho(2α4n)	25.6 min	5^{+}	645.25	16.20
^{160m}Ho(2α4n)	5.02 hrs	2^{-}	645.25	16.20
			728.18	30.8
			879.39	20.2

[a] these intensities are relative.

3 Obtained results & their interpretation

The EFs of ^{167}Lu(3n), ^{168}Lu(4n), ^{166}Lu(6n), ^{167}Yb(p3n), ^{165}Tm(α2n), ^{163}Tm(α4n), ^{161}Ho(2α2n), and ^{160}Ho(2α3n) radio-nuclides expected to be populated via CF and/or ICF of ^{13}C with ^{159}Tb have been measured in the energy range $\approx$ 4-7 AMeV. Information regarding the reaction mechanism in the ^{13}C+^{159}Tb interactions may be obtained by comparing the experimentally measured EFs to the theoretical ones. In the present work, the theoretical calculations have been performed using code PACE4[31] to check whether the reaction products are populated only via CF process. The code PACE4, which is a revised version of PACE2, is based on Hauser-Feshbach theory of CN-decay, uses statistical approach of CN de-excitation by Monte Carlo procedure. The angular momentum projections are calculated at each stage of de-excitation, which enables the determination of angular distribution of the emitted particles. The angular momentum conservation is explicitly taken into account. The code uses the BASS formula for CF cross sections calculation[32]. The default optical model parameters for neutron, proton and α-emission were used in the code. The γ-ray strength functions for E1, E2 and M1 transitions were taken from tables of Endt [33]. This code has been modified to take into account the excitation energy dependence of level density parameter using the prescription of Kataria et al. [34]. In this code, the level density parameter $a(= A/K)$, is

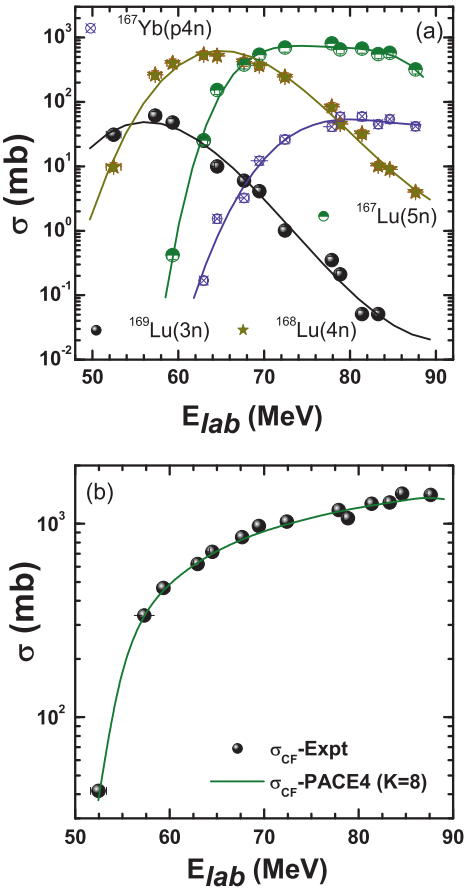

Fig. 2. (a) Experimental EFs of xn (x=3,4,5) and p4n-channels populated in the ^{13}C+^{159}Tb system. The solid lines through the data points are drawn to guide the eyes. (b) Sum of experimentally measured EFs of all xn/pxn-channels ($\Sigma\sigma_{CF}$) are compared with that predicted by PACE4 using physically reasonable parameters for mass-region A=150. Experimental data is in good agreement with the PACE4 calculations for a = A/8 MeV^{-1}.

one of the important parameters, where, A is the mass number of the nucleus and K is a free parameter. The value of K may be varied to match the experimental data. In the present work, a value of level density parameter (a) was taken as A/8 MeV^{-1} i.e. K=8 is used for the calculations as it gives best fit to the experimental data of complete fusion channels. It may, however, be pointed out that the ICF and PE-emission are not taken into consideration in this code.

3.1 xn and pxn-channels

Fig.2(a) shows the experimentally measured EFs of ^{169}Lu($t_{1/2}$=34.06 h), ^{168}Lu($t_{1/2}$=5.5 min, 6.7 min), ^{167}Lu($t_{1/2}$= 51.5 min), and ^{167}Yb($t_{1/2}$= 17.5 min) evaporation residues expected to be populated via 3n, 4n, 5n, and p4n emission from the excited ^{172}Lu* nucleus formed in CF reactions. Self explanatory notations are used to explain the decay channels in this figure. The solid lines through the data points are drawn to guide the eyes. During the decay-curve analysis, the evaporation residue ^{167}Yb(p3n) is found to be strongly fed from its higher charge isobar (pre-cursor here after) ^{167}Lu(5n) through β^{+}- emission. The half-life of of pre-cursor (i.e., $^{167}\mathrm{Lu} \rightarrow t^{pre}_{1/2} = 51.5$ min) is larger than the half-life of the daughter nuclei (i.e., $^{167}\mathrm{Yb} \rightarrow t^{d}_{1/2} = 17.5$ min). In this case, the independent production cross-section (σ_{ind}) of ^{167}Yb has been deduced using the following successive radio-active decay formulation [27];

$$N_d(t) = C_{t=0} \,.\, e^{-\lambda_d t} + \frac{(P_{pre} \,.\, \lambda_{pre})}{(\lambda_d - \lambda_{pre})} \,.\, N_{pre}(t) \,.\, e^{-\lambda_{pre} \,.\, t} \quad (1)$$

Where; $N_d(t)$ and $N_{pre}(t)$ are the number of daughter and pre-cursor nuclei produced at time 't'. $C_{t=0}$ is the cumulative (pre-cursor + daughter) number of nuclei produced at the end of the irradiation, σ_{pre} and σ_d are the production cross-sections of pre-cursor and daughter nuclei; and λ_{pre} and λ_d are the decay constants of pre-cursor and daughter nuclei, respectively. The value of $N_{pre}(t)$ has been deduced from the experimentally measured decay-curve of ^{167}Lu. The value of $N_d(t)$ (^{167}Yb) has been obtained by solving equation (1), which has been translated to its production cross-section (σ_{ind}), and is plotted in Fig.2(a) as independent production of $^{167}Yb^{(ind)}$(p4n).

Fig.2(b) shows the experimental EFs of all xn/pxn channels (i.e., $\Sigma\sigma^{exp}_{CF}$) compared with PACE4 predictions. As shown in this figure, the value of $\Sigma\sigma^{exp}_{CF}$ is very well reproduced by PACE4 for the level density parameter 'a' = A/8 MeV^{-1}, which is suitable for A=150 mass-region[11–14]. This indicates the production of these residues through the de-excitation of fully equilibrated compound nucleus formed in a CF reaction.

3.2 α-emitting channels

The experimental EFs of ^{166}Tm(α2n), ^{165}Tm(α3n), ^{163}Tm(α5n), ^{162}Ho(2α2n), ^{161}Ho(2α3n) and ^{160}Ho^{g+m}(2α4n) residues are shown in Fig.3(a). Due to the involvement of α-emission in the exit channel, these residues are expected to be populated via both CF and/or ICF processes. It has been noticed that the evaporation residue ^{165}Tm is strongly fed from its pre-cursor ^{165}Yb. In this case, the half-life of pre-cursor (i.e., $^{165}\mathrm{Yb} \rightarrow t^{pre}_{1/2} = 9.9$ min) is smaller than the daughter nuclei (i.e.,$^{165}\mathrm{Tm} \rightarrow t^{d}_{1/2} = 30.06$ hrs). Hence, the pre-cursor contribution has been subtracted using the prescription given by Cavinato *et al.* [27], and the deduced value of σ_{ind} of ^{165}Tm(α3n) is plotted in Fig.3(a).

Further, the sum of all identified α-emitting channels ($\Sigma\sigma^{exp}_{\alpha xn+2\alpha xn}$) is compared with that estimated by statistical model code PACE4 ($\Sigma\sigma^{PACE4}_{\alpha xn+2\alpha xn}$) in Fig.3(b). As can be seen from this figure, the experimentally measured EFs of αxn/2αxn - channels are significantly higher than PACE4 predictions for the

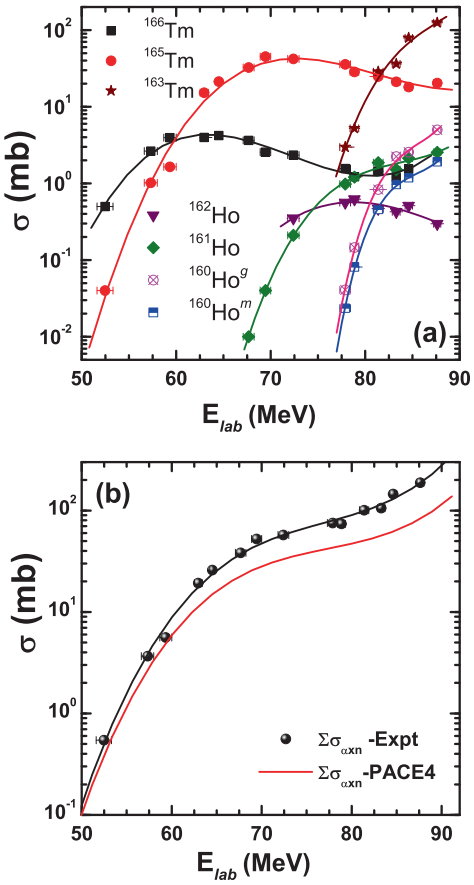

Fig. 3. (*a*) Experimentally measured excitation functions for all α-emitting channels are plteed. (*b*) The summed cross-section for all observed α-emitting channels and theoretically calculated production cross-sections of corresponding channels ($\Sigma\sigma_{\alpha xn/2\alpha xn}$) are plotted. The $\Sigma\sigma_{\alpha xn}$(expt) is significantly higher than that predicted by PACE4.

same set of parameter, which has been used to reproduce CF-residues in the present work. Since, the statistical model code PACE4 does not take ICF into account, therefore, the observed enhancement in the experimentally measured EFs over the theoretically predicted ones, points towards the contribution of ICF in the production of these residues. For example, the production of $^{165}Tm(\alpha 2n)$ via both CF and/or ICF can be justified as;

(i) CF: entire projectile (^{13}C) fuses with ^{159}Tb to form an excited CN (^{172}Lu*), which may decay through α3n or 2p5n channel leaving behind ^{165}Tm residual nucleus.

$$^{13}\text{C}+^{159}\text{Tb}\Rightarrow{}^{172}\text{Lu}^*\Rightarrow{}^{165}\text{Tm}+\alpha 3\text{n or 2p5n}$$

(ii) ICF: the projectile (^{13}C) breaks up into its constituent α-clusters (i.e., $^9Be+\alpha$). In this case, only a part of projectile (^9Be) fuses with ^{159}Tb to form an IFC system ($^{168}Tm^*$), while the remnant behaves like a spectator. The excited IFC system $^{168}Tm^*$ further decay through three neutrons (3n) to reach final reaction products ^{165}Tm.

$$^{13}C(^9\text{Be}+\alpha)\Rightarrow{}^9\text{Be}+^{159}\text{Tb}\Rightarrow{}^{168}\text{Tm}^*\Rightarrow{}^{165}\text{Tm}+\alpha\ (\text{spectator})+3\text{n}$$

In order to deduce ICF contribution in αxn/2αxn - channels, the same data reduction procedure has been used as given in refs.[11–13]. In recent reports [11–13], the fraction of ICF deduced using above data reduction procedure has been found to be in good agreement with that estimated from the analysis of forward ranges and angular distributions of heavy recoils. In order to see how does ICF contributes to the total fusion cross-section ($\sigma_{TF} = \Sigma\sigma_{CF} + \Sigma\sigma_{ICF}$), systematically deduced ICF cross-section ($\Sigma\sigma_{ICF}$) is plotted with the sum of all CF-channels ($\Sigma\sigma_{CF}$) and σ_{TF} as a function of projectile energy in Fig.4. As shown in this figure, the increasing separation between $\Sigma\sigma_{CF}$ and σ_{TF} with incident projectile energy indicates energy dependence of ICF.

4 Incomplete fusion strength function

As is evident from Figs.3 (b) & 4 that ICF-processes contribute significantly to the evaporation residue cross-sections. It can be noticed from Fig.4 that the CF component has significant contribution at ≈ 52 MeV projectile energy, while ICF contribution seems to start from ≈ 63 MeV. Further, it may also be noted from Fig. 4, that the separation between the plots for σ_{TF} and $\Sigma\sigma_{CF}$ increases with the projectile energy, which indicates larger contribution from ICF at relatively higher projectile energies. From Fig.4, it is clear that the ICF starts competing with CF from ≈ 20% above the Coulomb-barrier (V_b ≈ 52 MeV) and increases towards higher energies.

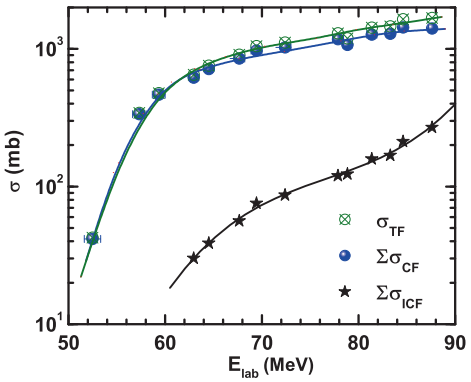

Fig. 4. The total fusion cross-section (σ_{TF}), the sum of all CF ($\Sigma\sigma_{CF}$), and ICF ($\Sigma\sigma_{ICF}$) channels are plotted as a function of incident projectile energy. Solid lines through the data points are drawn to guide the eyes. The value of $\Sigma\sigma_{ICF}$ significantly contributed to the value of σ_{TF}.

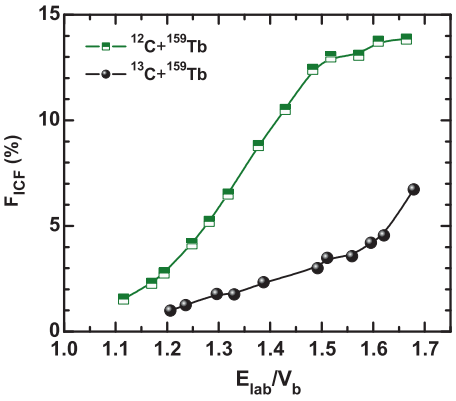

Fig. 5. The percentage fraction of ICF (F_{ICF}) for ^{12}C+^{159}Tb [14] and presently measured system ^{13}C+^{159}Tb are plotted as a function of reduced incident projectile energy (E_{lab}/V_b). The value of F_{ICF}smoothly increases with the projectile energy.

4.1 Dependence of F_{ICF} on projectile energy and α-Q-value

For better insights into the onset and influence of ICF, the percentage fraction of incomplete fusion (F_{ICF}) has been deduced from the analysis of data as demonstrated in ref.[11,12]. The F_{ICF} is a measure of relative strength of ICF to the total fusion, and defined

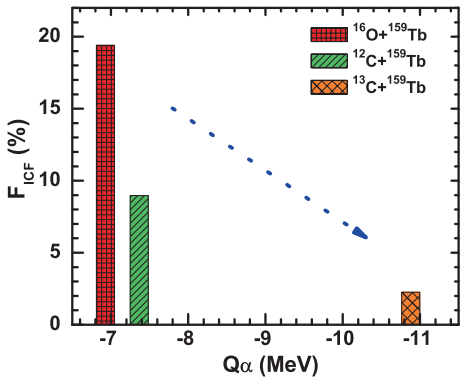

Fig. 6. The value of F_{ICF} for three different projectile combinations on same target at a constant v_{rel}=0.053 have been plotted against alpha-Q-value of the projectile.

as; F_{ICF} (%) = $(\Sigma\sigma_{ICF}/\sigma_{TF})\cdot 100$. The value of F_{ICF} is plotted as a function of reduced incident projectile energy (E_{lab}/V_b) in Fig.5, i.e., termed as ICF strength function.

The value of % F_{ICF} for two systems; (i) ^{13}C+^{159}Tb (present work) and (ii) ^{12}C+^{159}Tb [14] has been deduced using above formulation and is plotted as a function of reduced incident projectile energy in Fig.5. As can be seen from this figure, the value of F_{ICF}, for ^{13}C as projectile, is found to be $\approx$ 1.0 % at 1.20V_b (20 % above the barrier), and increases smoothly up to $\approx$ 7 % at highest measured energy (i.e., 1.68V_b). However, for ^{12}C+^{159}Tb system the F_{ICF} is found to be $\approx$ 1.5 % at 1.12V_b (12 % above the barrier), and increases smoothly up to $\approx$ 14 % at highest measured energy (i.e., 1.66V_b). From this figure it is evident that the ICF contribution for both the systems increases with the projectile energy, as expected.

It is not out of place to mention that the binding energy of ^{12}C is higher than the ^{13}C, however, it is surprising that though ^{12}C gives large ICF fraction. Hence, in order to ascertain this surprising picture, the F_{ICF} have been plotted against the alpha-Q-value of the projectile for the three different target-projectile combinations; ^{16}O+^{159}Tb, ^{12,13}C+^{159}Tb in Fig.6. From this figure it is evident that as the alpha-Q-value of the projectile increases, the F_{ICF} decreases. As such, the alpha-Q-value is a more reasonable parameter to understand ICF-reaction dynamics as compared to binding energy of the projectile.

5 Summary

In the present work, the EFs for several radio-nuclides produced via CF and/or ICF in ^{13}C +^{159} Tb interactions at energies $\approx$ 4-7 MeV/nucleon have been measured and analyzed in light of statistical model predictions. Some pxn and αxn-channels are found to be populated directly and/or via pre-cursor decay of higher charge isobar. An attempt has been made to deduce the independent production cross-section from cumulative and pre-cursor decay contribution of different radio-nuclides. The experimentally measured EFs have been found to agree reasonably well for xn/pxn-channels indicating their production via CF only, as expected. However, in case of all the α-emitting channels, significant enhancement in the production cross-sections has been observed as compared to theoretical model predictions and is attributed due to the ICF of ^{13}C i.e. the break-up of projectile into clusters (^{9}Be + ^4He and/or ^4He + ^{9}Be) leading to the various ICF processes. From the analysis it has, also, been observed that the projectile break-up probability increases with projectile energy, which reveals the dependence of ICF processes sensitively on projectile energy. The present results in light of the previously studied systems has concluded that the alpha-Q-value is an important parameter. As the alpha-Q-value increases the incomplete fusion contribution to total fusion decreases, which is justified. Further, it may also be concluded that apart from CF, the ICF is also found to contribute significantly to the total reaction cross-section even at projectile energies as low as $\approx$ 4-7 MeV/nucleon. Therefore, while predicting the total reaction cross-section for a projectile-target combination, the contribution from ICF should also be taken into consideration. Further, the better insight of underlying processes can be obtained by comparing a rich set of experimental data for various projectile-target combinations. However, the measurement of recoil range distribution and spin-distribution of residues populated by CF as well as ICF using particle-γ coincidence technique both at relatively low and higher bombarding energies may also provide a more clear and conclusive picture of the incomplete fusion processes.

6 Acknowledgments

The authors thank to the Director, IUAC, New Delhi, India, for providing all the necessary facilities to carry out the experiment and analysis. AY thanks to the UGC for providing financial support in the form of SRF. BPS and RP thank to DST and UGC for providing financial support.

References

1. H. C. Britt and A. R. Quinton, Phys. Rev. **124**, 877 (1961).
2. J. Galin et al., Phys. Rev. C **9**, 1018 (1974).
3. A. Diaz-Torres and I. J. Thompson, Phys. Rev. C **65**, 024606 (2002), Phys. Rev. Lett. **98**, 152701 (2007).

4. E. Z. Buthelezi, el al., Nucl. Phys. A **734**, 553-556 (2004).
5. P. R. S. Gomes, el al., Phys. Rev. C **73**, 064606 (2006), Phys. Lett. B **601**, 20 (2004).
6. M. Dasgupta, et al., Nucl. Phys. A, 787 (1), 144-149 (2007)
7. Pushpendra P. Singh, et al., Phys. Rev. C **77**, 014607 (2008); Euro. Phys. J. A **34**, 29-39 (2007), Phys. Rev. C **78**, 017602, and the references therein.
8. Pushpendra P. Singh, et al., Phys. Lett. B**671**, 20-24 (2009) and references therein.
9. Pushpendra P. Singh, et al., Phys. Rev. C**80**, 064603 (2009) and references therein.
10. Abhishek Yadav, et al., Euro. Jour. of Phys. Accepted.
11. Unnati Gupta, et al., Nucl. Phys. A **811**, 77-92 (2008), Phys. Rev. C**80**, 024613 (2009).
12. Devendra P. Singh, et al., Phys. Rev. C**80**, 014601 (2009) and references therein.
13. Devendra P. Singh, et al., Phys. Rev. C**81**, 054607 (2010).
14. Abhishek Yadav, et al., Phys. Rev. C (2011) communicated.
15. L. F. Canto, et al., Phys. Rev. C **58**, 1107 (1998).
16. M. Dasgupta, el al., Phys. Rev. C **70**, 024606 (2004).
17. L. Kowalski et al., Phys. Rev. **169**, 894 (1968).
18. J. R. Wu and I. Y. Lee, Phys. Rev. Lett. **45**, 8 (1980).
19. T. Udagawa and T. Tamura, Phys. Rev. Lett. **45**, 1311 (1980).
20. R. Weiner, M. Westrom, Nucl. Phys. A **386**, 282 (1977).
21. K. Siwek-Wilczynska, et al., Phys. Rev. Lett. **42**, 1599 (1979).
22. J. Wilczynski, et al., Nucl. Phys. A **373**, 109 (1982); Phys. Rev. Lett. **45**, 606 (1980).
23. T. Udagawa and T. Tamura, Phys. Rev. Lett. **45**, 1311 (1980).
24. J. R. Wu, and I. Y. Lee, Phys. Rev. Lett. **45**, 8 (1980).
25. J. Wilczynski, et al., Phys. Rev. Lett. **45**, 606 (1980); Nucl. Phys. A **373**, 109 (1982).
26. H. M. Morgenstern, et al., Phys. Rev. Lett. **52**, 1104 (1984); Z. Phys. A **313**, 39 (1983); Phys. Lett. **113B**, 463 (1982).
27. M. Cavinato, et al., Phys. Rev. C **52**, 2577 (1995).
28. CANDLE-Collection and Analysis of Nuclear Data using Linux nEtwork, B. P. Ajith Kumar et. al., DAE **SNP**, 2001, Kolkotta.
29. E. Browne, R.B. Firestone, Table of Radioactive Isotopes, Wiley, New York, 1986.
30. Firestone R B and Shirley V S (ed) 1996 Table of Isotopes 8th edn (New York: Wiley).
31. A. Gavron, Phys. Rev.C **21**, 230 (1980).
32. R. Bass, Nucl. Phys. A **231**, 45-63 (1974).
33. P.M. Endt, At. Data Nucl. Data Tables **26**, 47 (1981).
34. S. K. Kataria, V. S. Ramamurthy, S. K. Kapoor, Phys. Rev. C **18**, 549 (1978).
35. N. Patronis, et al., Phys. Rev. **C 75**, 034607 (2007).